UC Davis

UC Davis Previously Published Works

Title

CLASSIFYING THE UNDRAINED CYCLIC RESPONSE OF BIOCEMENTED SANDS

Permalink

https://escholarship.org/uc/item/0p93q13n

Journal

Biogeotechnics

ISSN

2949-9291

Authors

Luna, Laura MC

Boulanger, PE Ross W

Ziotopoulou, PE Katerina

et al.

Publication Date

2026-08-01

DOI

10.1016/j.bgtech.2026.100264

Peer reviewed

eScholarship.org Powered by the California Digital Library
University of California

Biogeotechnics xxx (xxxx) xxx

Contents lists available at ScienceDirect

Biogeotechnics

journal homepage: www.keaipublishing.com/en/journals/biogeotechnics/



Classifying the undrained cyclic response of biocemented sands

Laura M.C. Luna[a,*], Ross W. Boulanger[b], Katerina Ziotopoulou[b], Jason T. DeJong[b]

[a] Department of Civil and Environmental Engineering, Utah State University, Logan, UT 84322, United States
[b] Department of Civil and Environmental Engineering, University of California, Davis, CA 95616, United States

ARTICLE INFO

Keywords:
Biocementation
Microbially induced calcite precipitation (MICP)
Liquefaction mitigation
Constitutive modeling
Cemented sands

ABSTRACT

As biocementation technologies approach field-scale implementation, systematic frameworks for anticipating and classifying the cyclic response of treated soil across a range of cementation levels and loading conditions become increasingly valuable. This paper presents a behavioral classification framework for biocemented sands, informed by the cyclic stress path responses of MICP-treated Ottawa F65 sand subjected to constant-volume monotonic and cyclic direct simple shear (DSS) loading. Four distinct types of cyclic stress path response are identified: Type I (uncemented-like response), Type II (dilative-dominant behavior), Type III (clear evidence of bond breakage), and Type IV (high-cycle fatigue behavior). The conditions under which each behavior type is observed are formalized through quantitative boundaries in terms of V_{sR1} and CSR, where V_{sR1} is a stress-normalized shear wave velocity ratio reflecting the cementation level and CSR is the applied cyclic stress ratio. As an illustrative example, the framework is applied to evaluate the element-level performance of a plasticity constitutive model for lightly to moderately cemented sands for use in earthquake engineering applications.

Introduction

Since the late 1970s, there has been sustained interest in quantifying and predicting the mechanical behavior of naturally or artificially cemented sands under monotonic and cyclic loading (Clough et al., 1989; Frydman et al., 1980; Saxena & Lastrico, 1978). Cementation modifies soil behavior through three primary mechanisms of improvement: the formation of interparticle bonds at particle-to-particle contacts, infilling of void space, and coating of particle surfaces (DeJong et al., 2022). These mechanisms collectively lead to macroscopic changes in the stiffness, strength, dilatancy, and compressibility characteristics of cemented sands, which have been extensively quantified in previous laboratory studies (e.g., Abdulla & Kiousis, 1997; Ali Rahman et al., 2018; Consoli et al., 2012; Cuccovillo & Coop, 1999; Festugato et al., 2021; Lade & Overton, 1989; Porcino & Marcianò, 2017; Rasouli et al., 2020; Sharma & Fahey, 2004; Vranna & Tika, 2020).

Over the past decade, biocementation strategies such as microbially induced calcite precipitation (MICP) have emerged as promising ground improvement techniques for mitigating liquefaction-related hazards. Their potential has been widely demonstrated through laboratory and centrifuge studies (Burbank et al., 2013; Darby et al., 2019; Lee & Gomez, 2024; Lee et al., 2022; Lin et al., 2016; Montoya et al., 2013; Montoya & DeJong, 2015; Riveros & Sadrekarimi, 2020; San Pablo et al., 2024; Yu et al., 2024; Zamani et al., 2021). Collectively, the body of experimental work on naturally cemented, artificially cemented, and biocemented sands has underpinned the development of several constitutive models for cemented sands, including elasto-plastic models (Gai & Sánchez, 2019; Gao & Zhao, 2012; Nova et al., 2003), hypoplasticity models (Liao et al., 2024), bounding surface plasticity approaches (Rahimi et al., 2018; Zhang & Zhang, 2024), as well as discrete element methods (Zhang & Dieudonné, 2023; Zhao et al., 2025).

As biocementation continues to mature as a ground improvement technique and moves toward field-scale implementation, organizing and synthesizing the rich body of experimental observations into a framework for understanding and anticipating cemented soil response in terms of field-measurable parameters becomes increasingly valuable. This paper presents a behavioral classification framework for cemented sands, informed by the cyclic stress path responses of MICP-treated Ottawa F65 sand subjected to constant-volume monotonic and cyclic DSS loading. Four distinct behavior types are identified and described, and the conditions under which each is expected are established through quantitative boundaries as a function of cementation level and applied cyclic stress ratio. As an illustrative example, the classification

Peer review under the responsibility of Editorial Board of Biogeotechnics.
* Corresponding author.
E-mail address: laura.luna@usu.edu (L.M.C. Luna).

https://doi.org/10.1016/j.bgtech.2026.100264
Received 28 November 2025; Received in revised form 2 August 2026; Accepted 3 August 2026

2949-9291/© 2026 The Authors. Publishing services by Elsevier B.V. on behalf of KeAi Communications Co. Ltd. This is an open access article under the CC BY license (http://creativecommons.org/licenses/by/4.0/).

Please cite this article as: L.M.C. Luna, R.W. Boulanger, K. Ziotopoulou et al., Classifying the undrained cyclic response of biocemented sands, Biogeotechnics, https://doi.org/10.1016/j.bgtech.2026.100264

framework is then applied to evaluate the element-level performance of a plasticity constitutive model for sands at low to moderate cementation levels in earthquake engineering applications. The framework is intended as a transferable tool to anticipate the cyclic stress path response of cemented specimens at known cementation levels and applied loading, to evaluate the performance of proposed constitutive models across the range of relevant behaviors, and to guide future experimental, numerical, and design applications involving cemented soils.

Overview of experimental datasets

The experimental dataset considered in this study, illustrated in Fig. 1A, comprises results from direct simple shear (DSS) testing programs conducted at the University of Washington on biocemented Ottawa F65 sand specimens. The full experimental results are documented in three publications: one focusing on low biocementation levels (Lee et al., 2022), another focusing on low to moderate cementation levels tested across a wider range of cyclic stress ratios (Lee & Gomez, 2024), and a dissertation compiling all available results (Lee, 2022). The publications also include tests on uncemented Ottawa F65 specimens across a wide range of relative densities, which serve as the baseline for evaluating the progressive effects of biocementation on observed responses. The present study considers the constant volume (i.e., equivalent undrained) strain-controlled monotonic and stress-controlled cyclic DSS tests on biocemented specimens, which together underpin the development of the behavioral classification framework.

All tests were performed using an electromechanical dynamic cyclic simple shear (EMDCSS) device manufactured by GDS Instruments, using a stack of low-friction steel rings providing lateral confinement. Specimen preparation involved dry pluviation of Ottawa F65 sand into a latex membrane to achieve a loose relative density ($D_r \approx 30\%$), preconditioning protocols (Humire et al., 2022), saturation with de-aired water, consolidation to a vertical effective stress of $\sigma'_{vc} = 100$ kPa, and biocementation treatment. Biocementation was conducted using microbially induced calcite precipitation (MICP), through sequential injection of augmentation solutions containing *Sporosarcina pasteurii* and calcium-enriched cementation solutions. The level of cementation was monitored through shear wave velocity (V_s) measurements obtained via bender-extender element sensors embedded in the end platens. Equivalent undrained conditions were maintained using active height control. Monotonic tests involved strain-controlled shearing at rates of 0.05% or 0.1% per minute; cyclic tests involved unidirectional sinusoidal stress-controlled loading at frequencies between 0.005 and 0.05 Hz. Further experimental procedures and detailed results are documented in the original publications.

In this study, cementation level is quantified through the stress-normalized shear wave velocity ratio, V_{sR1}, defined as the ratio of the cemented to uncemented shear wave velocity (V_{sR}) at a reference vertical effective stress of $\sigma'_{vc} = 101.325$ kPa (Luna, Ham, et al., 2026). The original publications quantify cementation level in terms of ΔV_s, the difference between cemented and uncemented V_s. V_{sR1} is adopted here in lieu of ΔV_s because (1) ratio-based metrics simplify formulations involving mechanical properties because elastic shear modulus scales with the square of V_s, and (2) stress normalization renders the metric independent of the stress level at which measurements are obtained, which is desirable for its use as a state variable.

The relationship between ΔV_s and V_{sR} is given by:

$$V_{sR} = 1 + \Delta V_s / V_{s,unc} \quad (1)$$

where $V_{s,unc}$ is the V_s of the specimen prior to biocementation treatment but after consolidation. Since all specimens in this study were consolidated to $\sigma'_{vc} = 100$ kPa, no stress correction is required and $V_{sR1} = V_{sR}$. Fig. 1B and C display the measured cemented and uncemented V_s for each specimen in the dataset, showing that $V_{s,unc} \approx 150$ m/s is a representative value which yields a good approximate conversion between ΔV_s values from the original publications and the V_{sR1} values reported in this study.

Observed behaviors during cyclic DSS loading

Examination of the stress path responses across the dataset reveals four consistent patterns of behavior. These behaviors range from responses qualitatively similar to those of uncemented sands at low cementation levels to behaviors dominated by strong dilation and clear evidence of bond breakage at higher cementation levels and cyclic stresses. A single-amplitude shear strain of 3% is adopted as the criterion for cyclic strength mobilization (and thus failure). While the biocemented specimens do accumulate high excess porewater pressures ($r_u \approx 1$) and develop large shear strains ($\gamma_{SA} > 3\%$) during testing, the term liquefaction is not used here because it can also encompass phenomena such as flow liquefaction and field surface manifestations that are not the focus of this study. The following observations are made for each behavior type.

Type I: uncemented-like response

At low cementation levels (i.e., $V_{sR1} < 2$), tests that failed within 100 cycles exhibit stress path patterns akin to those of uncemented sands. The criterion for Type I behavior is: if only a plot of the stress path is provided, without additional information on the specimen's cemented state, would it be apparent that the tested material differs from a typical loose uncemented sand? If the answer is no, then the test is classified as Type I.

Fig. 2A–D show an example test exhibiting Type I behavior. The stress path response, shown in Fig. 2B, starts at the applied stress of $\sigma'_{vc} = 100$

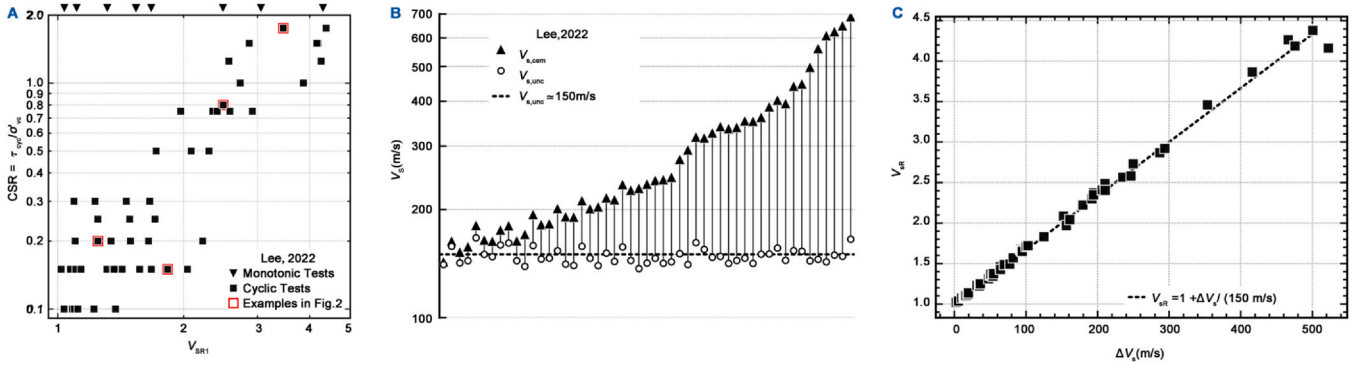


Fig. 1. (**A**) Cyclic and monotonic constant-volume DSS tests on MICP-treated Ottawa F65 sand specimens (Lee, 2022), shown in terms of cementation level and applied cyclic stress ratio. Illustrative examples shown in Fig. 2 are highlighted in red; Shear wave velocity measurements obtained via bender-extender elements embedded in the DSS device end-platens (Lee, 2022), showing (**B**) cemented ($V_{s,cem}$) and uncemented ($V_{s,unc}$) velocities for each specimen under $\sigma'_{vc} = 100$ kPa, and (**C**) conversion between ΔV_s and V_{sR} for this dataset.

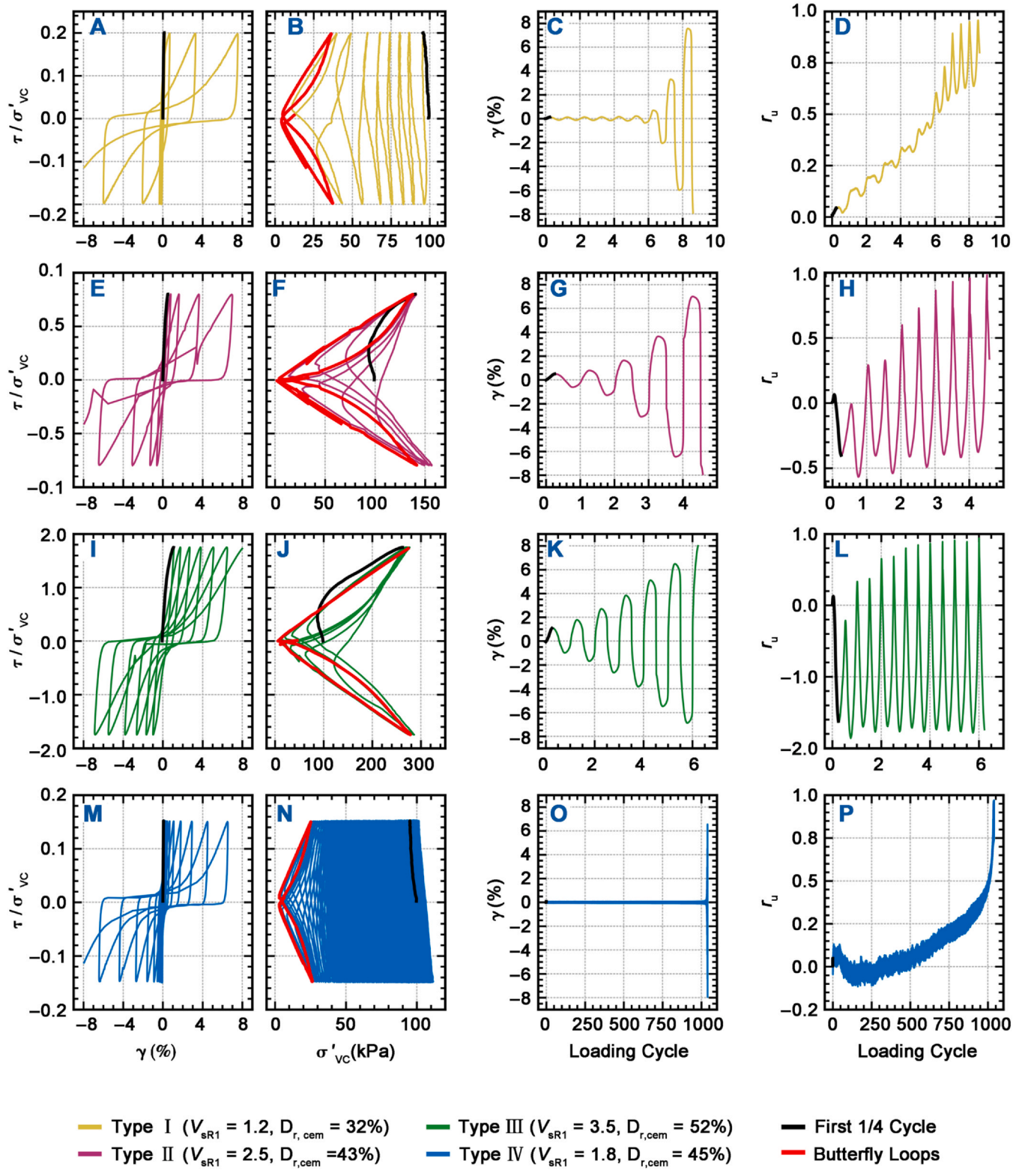


Fig. 2. Illustrative examples of the four types of responses observed in MICP-treated Ottawa F65 specimens (Lee, 2022), showing for each type: (**A**,**E**,**I**,**M**) Stress-strain response; (**B**,**F**,**J**,**N**) Stress path; (**C**,**G**,**K**,**O**) Shear strain versus loading cycle; and (**D**,**H**,**L**,**P**) excess pore pressure ratio ($\Delta u/\sigma'_{vc}$) versus loading cycle.

kPa with the initial loading (black) inducing a contractive response that causes a small reduction in effective stress. Upon load reversal and subsequent cyclic loading, σ'_v progressively decreases until the traditional "*butterfly*" loop pattern emerges with $\sigma'_v = 0$ developing transiently when the applied shear stress is zero. Fig. 2D shows the corresponding buildup of excess pore water pressure throughout the test, represented through the excess pore water pressure ratio ($r_u = \Delta u/\sigma'_{vc}$), versus the number of loading cycles. There is a gradual increase in pore water pressure as cyclic loading progresses until reaching $r_u > 0.9$, at which point each full loading cycle follows a *W* pattern that mirrors the contraction and dilation observed in the *butterfly* loop portion of the stress path (red). The peaks of the *W* pattern correspond to when the applied shear stress is near zero

while the troughs occur as the peak CSR is mobilized (in this case, CSR = 0.2), due to a dilative response.

Although the stress path patterns resemble those of uncemented sands, these tests differ in that the number of cycles to failure is substantially greater than typical for an uncemented sand under comparable testing conditions. This is evident in both a slower r_u accumulation and a delayed onset of large shear strains. For example, while an uncemented sample of Ottawa F65 sand with D_r = 32% would be expected to fail within one cycle of CSR = 0.2 loading (Lee & Gomez, 2024), the cemented sample in Fig. 2 required 7 loading cycles to failure under similar testing conditions.

Type II: dilative-dominant behavior

As V_{sR1} and CSR increase, the observed stress paths diverge from the typical behavior of uncemented sands. Compared to their uncemented counterparts, cemented sands can sustain larger applied CSR before sustaining significant shear strains. When tested under these higher CSR values (i.e., CSR > 0.5), early loading cycles mobilize shear stress sufficiently large to manifest a phase transformation response, with an initial contractive response being followed by strongly dilative behavior in each loading cycle. The presence of these strongly dilative tendencies in early loading cycles distinguishes this behavior from the earlier *Type I: uncemented-like response*, where phase transformation does not occur until the later stages of loading once a significant reduction in effective stress has occurred.

Fig. 2F exemplifies this type of response, with the initial positive loading cycle (black) initially mildly contracting from the initial state (σ'_{vc} = 100 kPa) to a lower confining stress of σ'_v = 90 kPa, but then transitioning to a dilative behavior at a shear stress ratio $\tau/\sigma'_{vc} \approx 0.3$. When reaching the reversal stress criterion at a CSR of 0.85, the strong dilative response has increased σ'_v to 140 kPa. During unloading, a strong counteracting contractive response occurs, shedding the gained effective stress and returning it to near the starting level. This cycle of alternating contractive and dilative behavior within individual positive loadings forms a pattern that resembles the *butterfly* loops that manifest in uncemented sands after ($r_u \approx 1$) has been triggered, albeit with reduced concavity as the effective stress at the end of each loading cycle (i.e., at $\tau/\sigma'_{vc} \approx 0$) remains relatively large. As cyclic loading continues, strain-induced damage gradually breaks down the brittle cementation bonds, reducing the dilative tendencies of the material. This breakdown results in a progressive reduction of effective stress at the end of each loading cycle, eventually leading to a *butterfly* loop response consistent with uncemented soils.

The development of excess pore water pressures (Fig. 2H) mirrors the patterns observed in the stress path. Each positive loading results in a slight increase in r_u followed by a steep decrease towards negative values (up to $r_u = -0.5$), whereas reversal loadings return the r_u values to be initially near zero and then progressively increase towards $r_u = 1$. In Fig. 2H, the negative peaks in r_u correspond to the peak applied shear stresses whereas the positive r_u peaks correspond to the beginning stages of a loading cycle when crossing the phase transformation line (i.e., when transitioning from contractive to dilative behavior). The buildup of pore pressure follows the *W* pattern through the entirety of the test, with the positive peaks increasing from the initial condition ($r_u \approx 0$) towards a "liquefied" state ($r_u > 0.98$). This behavior is thus named *dilative-dominant* because most of the loading over time occurs when the material is under highly dilative tendencies and when transiently mobilizing negative excess pore pressures.

Type III: clear evidence of bond breakage

For samples tested at the highest range of cementation levels and cyclic stresses (i.e., $V_{sR1} > 2.5$ and CSR > 0.8), a distinction can be observed relative to the behavior described in Type II. Type III behavior differs in that the first loading cycle mobilizes greater stress obliquity (i.e., σ'_1/σ'_3, τ/σ'_v, or higher failure envelope) than during subsequent loading cycles. In the dataset, Type III is assigned whenever the first positive loading cycle reaches a higher failure envelope than is reached in the later *butterfly* loop pattern. As shown in Fig. 2, Type II and Type III behaviors are observed within a transition zone at intermediate cementation levels and cyclic stresses, which may be the result of a gradual physical transition or a reflection of experimental scatter.

An illustrative example is shown in Fig. 2J, in which the first loading cycle (black) mobilizes a peak $\tau/\sigma'_v > 1$ when σ'_v = 110 kPa, whereas subsequent loading cycles only mobilize $\tau/\sigma'_v \approx 0.7$ (i.e., the secant slope of stress paths). This pattern provides evidence of material destructuring that occurs due to the breakage of brittle cementation during applied loading. While the breakage of cementation bonds in lower cementation levels and CSRs is inferred from changes in volumetric tendencies or reductions in stiffness, the de-structuring of the material is more distinctly visible in this set of DSS tests.

Type IV: high-cycle fatigue behavior

Several samples with modest cementation levels (e.g., $V_{sR1} \approx 1.8$) subjected to lower cyclic loads (e.g., CSR ≈ 0.15) did not develop significant excess pore pressures or shear strains over the first 100 cycles but did eventually accumulate large excess porewater pressures ($r_u \approx 1$) and shear strains ($\gamma_{SA} > 3\%$) after 600–45,000 cycles. These tests illustrate the high-cycle fatigue behavior of cementation and provide valuable insights for constitutive model development.

Fig. 2M–P display an example of this behavior for a test that develops $r_u \approx 1$ after 1000+ cycles. The first 200 cycles resulted in small shear strain deformations and little to no accumulation of excess pore water pressures. Accordingly, the stress path oscillates vertically around the starting σ'_{vc} = 100 kPa and significant reductions in effective stress are not observed until more than 1000 cycles have occurred. Aside from the large number of cycles and associated delay in r_u buildup, the stress path resembles the general patterns described in Type I.

This set of tests highlights the high-cycle fatigue of biocementation, which can aid in constitutive model development and the understanding of how biocemented sands may respond to long-duration loadings (e.g., wind, wave, machine foundation vibrations). For constitutive model development, it is noted that Fig. 2O displays peak shear strains below 0.1% during the first 1000 cycles. Small-strain measurements in DSS devices are compromised due to compliance in the mechanical system; therefore, it is expected that the strains actually mobilized within the specimen are smaller than the reported values. This experimental limitation adds uncertainty to the use of this dataset for constraining relationships controlling high-cycle fatigue behavior.

Quantitative classification framework

Fig. 3A–B plot all the available cyclic DSS tests in V_{sR1} versus CSR space, with each test colored according to its assigned behavior type. A clear grouping emerges, with tests that exhibit the same behavior clustering in distinct regions of the space, suggesting that the cementation level and applied CSR jointly govern the type of response a specimen will exhibit. This observation motivates the development of boundary lines separating the four behavioral regions, which are described below.

Monotonic failure boundary

The uppermost boundary separates conditions under which specimens fail monotonically (i.e., within the first quarter cycle of a stress-controlled cyclic test) from those that can sustain at least one load reversal before failing. This boundary is derived from the strain-controlled monotonic DSS tests, since strain-controlled loading can capture the stress-softening response more reliably than stress-controlled loading. Fig. 3D shows the monotonic responses across a range of

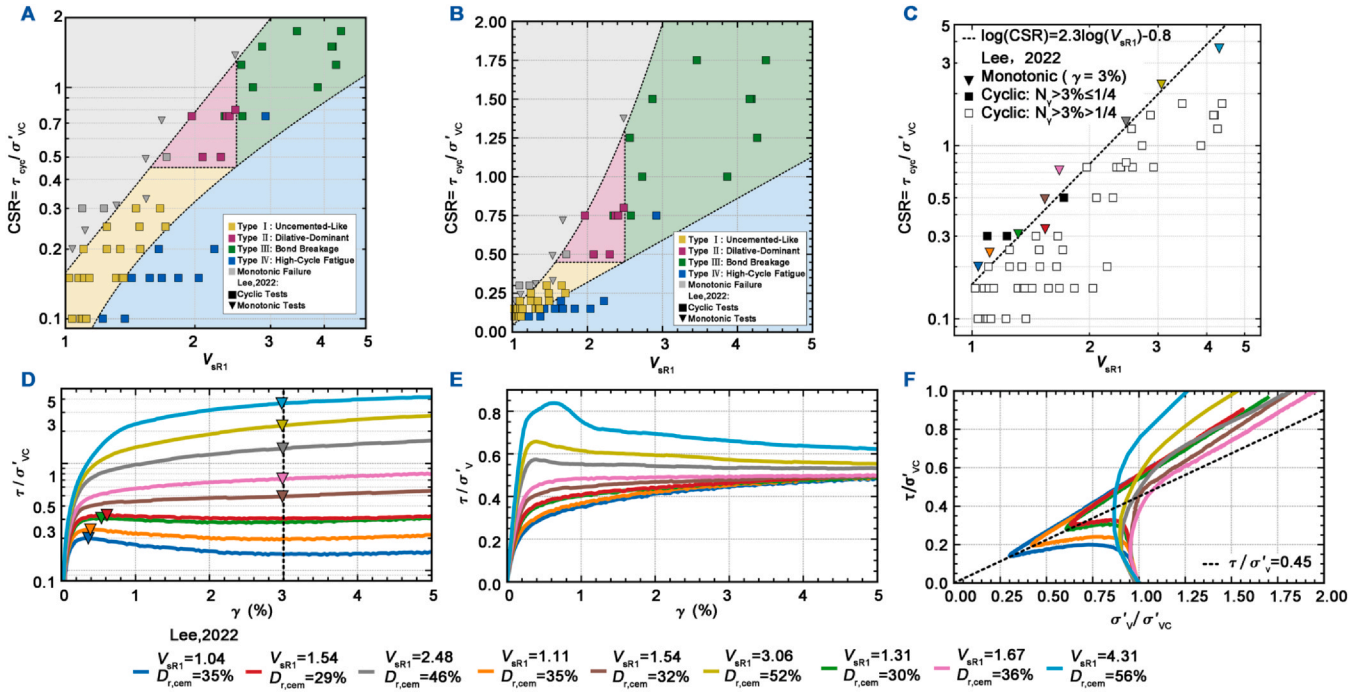


Fig. 3. Quantitative behavioral classification framework for MICP-treated sands under constant-volume cyclic DSS loading at σ'_{vc} = 100 kPa, shown in (**A**) log-log and (**B**) arithmetic scales. Dashed lines denote the boundaries between behavioral regions; colored squares indicate the assigned behavior type for each cyclic test; gray squares indicate cyclic tests that reached γ_{SA} = 3% within one quarter cycle; and gray triangles indicate the peak cyclic stress ratio mobilized by γ_{SA} = 3% in monotonic tests; (**C**) Monotonic failure boundary, showing the cyclic stress ratio at γ_{SA} = 3% as a function of V_{sR1} for monotonic DSS tests (Lee, 2022) with color coding following. The fitted boundary is shown as a dashed line. Cyclic tests that reached γ_{SA} = 3% within and beyond the first quarter cycle are also shown for reference; Strain-controlled monotonic constant-volume DSS responses of MICP-treated Ottawa F65 specimens at increasing cementation levels (Lee, 2022): (**D**) Shear stress ratio τ/σ'_{vc} versus shear strain, with markers indicating the point of γ_{SA} = 3%, (**E**) Mobilized stress ratio τ/σ'_{v} versus shear strain, (**F**) Normalized stress paths (τ/σ'_{vc} versus σ'_{v} /σ'_{vc}).

cementation levels ($1 < V_{sR1} < 5$). For consistency with the definition of CSR, the monotonic failure boundary is defined by the maximum shear stress mobilized prior to reaching γ_{SA} = 3%, normalized by the effective vertical stress at the end of consolidation (σ'_{vc} = 100 kPa).

Fig. 3C plots the corresponding CSR as a function of V_{sR1}, with the boundary being defined according to:

$$\log(CSR) = 2.3\log(V_{sR1}) - 0.8 \quad (2)$$

Cyclic tests that failed within the first quarter cycle cluster near this boundary, and all tests that failed in more than one quarter cycle plot correctly below it.

High-cycle fatigue boundary

The lowermost boundary separates specimens that develop significant shear strains within the first 100 loading cycles from those that maintain low shear strains (e.g., $\gamma_{SA} < 0.1\%$) before eventually failing at much larger cycle counts. This boundary was derived empirically from the available cyclic test results, with the boundary given by:

$$CSR = 0.27\,(V_{sR1} - 1) + 0.05 \quad (3)$$

This linear form was selected for its simplicity and reasonable fit to the available data. At V_{sR1} = 1 (uncemented condition), the boundary yields CSR = 0.05, generally consistent with the uncemented response of Ottawa F65 sand presented by Lee and Gomez (2024). As cementation increases, the boundary shifts upward, reflecting the increased resistance of cemented specimens to cyclic strain accumulation. The high-cycle fatigue regime corresponds to conditions where DSS device compliance may affect small-strain measurements, as discussed in the observed behaviors section. This boundary should therefore be interpreted as an approximate guide rather than a precise threshold.

Boundary between Type I and Type II behavior

For a specimen to exhibit Type II behavior, two conditions must be simultaneously satisfied: (a) the cementation level must be sufficient for the specimen to cross the phase transformation line without first reaching $\gamma_{SA} > 3\%$, and (b) the applied CSR must be large enough to induce crossing of the phase transformation line during the initial monotonic (or first quarter cycle of) loading.

Both conditions were examined using the monotonic stress-strain and stress path responses shown in Fig. 3(D–F), with the following observations: (a) strain-softening responses are observed up to V_{sR1} = 1.5, for which specimens exhibit a phase transformation response coincides with the development of large shear strains, and (b) the phase transformation line occurs at τ/σ'_{v} = 0.45, with more cemented specimens ($V_{sR1} > 1.5$) exhibiting small reductions in vertical effective stress prior to dilating. Under the conditions in this study (σ'_{vc} = 100 kPa), it follows that the applied CSR must exceed 0.45 to achieve phase transformation within the first quarter cycle. A Type II response requires both $V_{sR1} > 1.5$ and CSR > 0.45. Since the monotonic failure boundary is more restrictive than the V_{sR1} criterion, this phase transformation boundary plots solely as a horizontal line at CSR = 0.45 in Fig. 3(A–B).

Boundary between Type II and Type III behavior

This boundary separates specimens exhibiting dilative-dominant behavior from those showing clear evidence of bond breakage during the first loading cycle. Under the premise that the specimen is loaded under sufficiently large cyclic stresses, the observation of bond breakage is primarily governed by cementation level. As shown in Fig. 3E, the lowest cementation level exhibiting clear bond degradation during loading corresponds to V_{sR1} = 2.48. The cyclic data exhibit some

scatter near this boundary, with overlap between Type II and Type III specimens as discussed in the observed behaviors section. A boundary of $V_{sR1} = 2.5$ is adopted based on these observations. For $V_{sR1} > 2.5$, any specimen plotting above the fatigue boundary and below the monotonic failure boundary is expected to exhibit Type III behavior, as the corresponding CSR values are sufficiently large to mobilize bond breakage prior to the first load reversal.

Summary

The four boundaries described above define five regions in V_{sR1} vs. CSR space, four of which correspond to the behavior types identified in the preceding section and one corresponding to monotonic failure. For a specimen at a given V_{sR1} and applied CSR, the behavior type can be determined by sequentially evaluating the following conditions:

1) If CSR $>$ 10 ^ (2.3 log (V_{sR1}) – 0.8): monotonic failure
2) If CSR $<$ 0.27 (V_{sR1} – 1) + 0.05: Type IV, high-cycle fatigue
3) If $V_{sR1} > 2.5$: Type III, clear evidence of bond breakage
4) If CSR $>$ 0.45: Type II, dilative-dominant behavior
5) Otherwise: Type I, uncemented-like response

Illustrative application to constitutive model development

The behavioral classification framework developed in this study was applied to evaluate the element-level performance of PM4SandC (Luna, El Kortbawi, et al., 2026), a plasticity model for lightly to moderately cemented sands for earthquake engineering applications. This section presents one illustrative simulation per behavior type, demonstrating how the classification framework can be used to assess a constitutive model's ability to replicate the range of observed cyclic responses.

Constitutive model

The following provides a brief overview of the key modeling considerations relevant to replicating the four behavior types identified in the classification framework. PM4SandC builds on the PM4Sand model (Boulanger & Ziotopoulou, 2023) for uncemented sands and extends its formulation to accommodate behaviors observed in cemented materials. While the model is calibrated here based on results from MICP-treated Ottawa F65 sand, the formulation is intended to be applicable to other lightly to moderately cemented sands, provided the cementation-specific parameters are recalibrated to reflect the characteristics of the cementing agent and sand. The following mechanisms are relevant for reproducing the observed behavior types and therefore motivate the constitutive features included in PM4SandC:

1. *Cementation Level.* Cementation is quantified through V_{sR1}, which corresponds to the ratio of cemented to uncemented shear wave velocity that would have been measured at a vertical effective stress of 101.325 kPa. A V_s-based measure of cementation is preferred over measures of cement content (such as percent calcite by mass), because V_s measurements will enable the model to be used more broadly for other cemented sand conditions, occurring either naturally or due to other ground improvement techniques. In addition, V_s measurements are already common in site investigations for earthquake engineering projects and the ability to readily measure 2D profiles using geophysical methods allows for a more comprehensive assessment of the spatial variability across a site. The model uses a stress-corrected measure because V_s-based metrics of cementation are dependent on the level of stress at which they are taken.
2. *Increased Peak Shear Strength.* Cemented sands have higher failure envelopes in both drained and undrained loading. To capture this behavior, the constitutive model space is shifted by a mean effective stress Δp, correlated to the additional bonding strength afforded by cementation bonds. This strategy is common with earlier constitutive models for structured materials (e.g., Gai & Sánchez, 2019; Gao & Zhao, 2012; Nova et al., 2003; Rahimi et al., 2018).
3. *Increased Stiffness*. Accurately modeling the stiffness profile at a site is crucial for seismic wave propagation problems. Cemented sands not only have an increased stiffness, but also a reduced dependency between the shear modulus and the confining stress. In PM4SandC, the stiffness is calibrated to measured shear wave velocity data using the dimensionless cemented shear modulus coefficient, $G_{o,cem}$ and the shear modulus stress exponent (typically 0.5 for uncemented sands) is reduced by a value Δn. Finally, because highly cemented sands have some stiffness even when fully unconfined, the shear modulus is calculated using the modified effective stress space, corresponding to the mean effective stress plus Δp.
4. *Increased Dilatancy*. Biocemented sands exhibit larger incremental volumetric deformations under drained shear loading compared to uncemented sands. This increased dilative tendency is important under both drained and undrained loading conditions, making it crucial to accurately model the pronounced dilative and contractive tendencies observed in Type II and Type III stress paths. In PM4Sand, dilatancy is calculated based on Bolton's dilatancy relationship (Bolton, 1986). In PM4SandC, an additional dilatancy component (calibrated through the parameter C_ψ) is introduced to account for and track the presence and eventual degradation of the cementation bonds.
5. *Strain-Induced Bond Degradation.* A crucial aspect of modeling the behavior of cemented sands is capturing the degradation of bonds as mechanically induced damage accumulates. As cementation bonds break under applied loading, the mechanical behavior progressively weakens. After significant straining, the behavior of cemented sands can largely collapse back to that of uncemented materials. Degradation rules are incorporated into the model to account for this progressive de-structuring. The model employs an accumulation function (with calibration parameters: γ_t, and β) and a degradation function (with two calibration parameters: γ_{rs} and γ_{pk}). This approach allows, for example, the modeling of Type III behavior, where early cycles mobilize higher stress ratios than subsequent cycles. $V_{sR1}$is employed as a unifying metric, ensuring that the degradation of cementation effects occurs at relative rates proportional to the anticipated relationships between parameters.
6. *Increased Cyclic Strength.* The above modifications to the model (increased stiffness, peak monotonic strength, and dilatancy) automatically yield a material with a higher cyclic strength. Final fine-tuning of the cyclic resistance ratio (CRR) is controlled by the contraction rate parameter, h_{po} (as is typical for the parent model PM4Sand) and by the rate of bond degradation.

Element-level simulation approach and results

The ability of PM4SandC to model the behavior types observed in the DSS dataset is assessed here by completing element-level simulations of the illustrative examples highlighted in Figs. 1A and 2. Single element simulations are initiated under a vertical effective stress of 100 kPa, a $K_o = 0.5$ condition, and then subjected to shear loading under constant volume conditions analogous to the cyclic loading applied in the DSS test.

The parameter selection for each simulation is summarized in Table 1, with other secondary input parameters being left at the default values specified in the PM4Sand user manual (Boulanger & Ziotopoulou, 2023). These represent individual calibrations performed to match the behaviors observed in the illustrative DSS tests, intended solely to demonstrate that PM4SandC can replicate these responses. Calibrations for use in system-level nonlinear dynamic analyses require evaluating a broader collection of behaviors (e.g., monotonic drained and undrained response, modulus reduction and damping curves, etc.), with the relative importance of each depending on the governing

Table 1
Selected PM4SandC input parameters for element-level simulations.

V_{sR1}	D_r (%)	$G_{o,unc}$	Δp (kPa)	Δn	c_ψ	z_{max}	ϕ_{cv} (^{o})	γ_{pk} (%)	γ_{rs} (%)	γ_t (%)	n^d	h_o	β	h_{po}
1.2	32	530	1	0.05	0.57	5	30	1	8	4	2	0.25	10	3
2.5	52		14	0.25		23	32	0.1	8	4		0.15	1	10
3.5	43		45	0.30		25	34	0.1	20	10		0.10	6	10
1.8	45		5	0.15		22	31	1	8	4		0.25	2.28	5

deformation mechanisms. Calibrations of the PM4Sand model considering these factors and a suggested calibration procedure are presented in Luna, El Kortbawi, et al. (2026).

Fig. 4 compares the results from element-level simulations against the experimental DSS test results. Overall, the simulations display an ability to reproduce the measured stress path responses. For Type I behavior, r_u accumulation within the first cycle is slightly overestimated by the model, but the subsequent rate of accumulation and *W* pattern are captured well. The stress-path matches the progressive reduction in vertical effective stress throughout loading and the *butterfly* pattern. The shear strains are also well approximated, leading to a stress-strain response that matches quite well with the experimental results.

Modeling Type II and III behaviors is enabled by the changes in constitutive model formulation, particularly the increased dilative tendencies that occur due to cementation bonds. The transition from contractive to dilative response within each loading cycle is well captured, with the simulations following a similar stress path as the DSS test result. The patterns of pore water pressure accumulation in the simulations (Fig. 4H and 4L) match the *W* pattern observed experimentally. A challenge associated with modeling these responses is that the model's plastic modulus upon reversal in early loading cycles is large, since the stiffness is proportional to the stress-ratio distance to the last reversal and fabric effects have not yet accumulated. As a result, the simulation stress paths are vertical upon early load reversal, whereas the DSS tests exhibit an immediate highly contractive response. This is mirrored in the r_u plots, leading to troughs of the *W* pattern being wider in the simulation than in the experiments. The difference is eliminated once fabric effects have accumulated, with later loading cycles in the simulation better matching the experimental results. This difference is minimal in the context of modeling the overall soil response.

The post-failure ($\gamma_{SA} > 3\%$) strain accumulations in the simulations are larger than those observed experimentally. Even after significant breakage of cementation bonds, the DSS results on biocemented specimens indicate a slower post-failure ($\gamma_{SA} > 3\%$) shear strain accumulation when compared to uncemented sands. In the simulated responses, cementation has largely degraded once $\gamma_{SA} > 3\%$ is reached.

In Type IV, the simulated response to the first 1000 cycles reasonably predicts low levels of strains in response to the applied loading. At larger cycle numbers (i.e., $N > 1100$), the model can capture the eventual breakdown of fabric and allows for the development of larger shear strains. There is a drop in vertical effective stress and corresponding buildup of $r_u$in the first few cycles that is not observed in the experimental test result. This vertical effective stress reduction is associated with an early increase in K_o during the simulation and not with any contractive tendencies of the element itself. As the soil element is loaded plastically in these first few cycles, the K_o condition progressively increases to $K_o = 1.0$ (a common feature of plasticity models), which induces a drop in vertical effective stress and increase in horizontal effective stress during undrained shearing. In the next 100 cycles, further buildup of pore pressures occurs as the material is loaded below the dilatancy surface. Once the stress state crosses above the dilatancy surface, the r_u value stabilizes until degradation of the bonds eventually allows for the accumulation of large shear strains and large excess pore pressures in upwards of 1000 cycles.

Discussion

This paper presents a behavioral classification framework for lightly to moderately biocemented sands, based on experimental results from MICP-treated Ottawa F65 sand subjected to constant-volume cyclic DSS loading. Four distinct types of stress path response were identified across a range of cementation levels and applied cyclic stress ratios. The framework is formalized through quantitative boundaries in V_{sR1}-CSR space, derived from monotonic and cyclic DSS test results at $\sigma'_{vc} = 100$ kPa. By organizing experimental observations into distinct behavioral categories with defined boundaries, the framework provides a transferable tool for three purposes: (1) anticipating the cyclic response of biocemented specimens at known cementation levels and applied loading; (2) evaluating the performance of proposed constitutive models across the range of relevant behaviors; and (3) guiding future experimental, numerical, and design applications involving biocemented soils.

Some limitations of the classification framework should be noted. First, the boundaries were established using a single sand type (fine-grained, poorly graded Ottawa F65 sand) treated via MICP under a single consolidation stress ($\sigma'_{vc} = 100$ kPa). The location of the boundaries in V_{sR1}-CSR space may shift with consolidation stress, sand type, and cementation process, and such effects warrant further investigation. Second, the high-cycle fatigue boundary was derived empirically from a limited number of tests, and DSS device compliance affects small-strain measurements in this regime; this boundary should therefore be interpreted as an approximate guide rather than a precise threshold. Third, the Type II to Type III transition exhibits some scatter, reflecting either a gradual physical transition or experimental scatter around a sharper boundary; additional testing near this boundary would help disambiguate these interpretations.

While the framework was developed for MICP-treated Ottawa F65 sand, the four behavior types identified are expected to be broadly relevant to other lightly to moderately cemented sands, as they are governed by the same underlying mechanical phenomena: strain-induced bond degradation, increased dilative tendencies due to cementation, and the progressive transition from cemented to uncemented-like behavior as bonds break down under loading. These phenomena are common across biocementation strategies that produce similar cementing agents, such as other biogeochemical pathways, as well as naturally cemented sands where carbonate or similar cementing agents are present. The specific location of the boundaries, however, is expected to depend on the characteristics of the cementing agent, the base sand properties, and the consolidation stress level. Extending the framework to other sands, cementation methods, and stress levels represents a natural direction for future work, and the V_{sR1}-based metric is well suited for this purpose given its broad applicability to cemented materials and its compatibility with standard site investigation methods.

As an illustrative example of one application of the framework, the behavioral classification was used to evaluate the performance of PM4SandC, a plasticity constitutive model for lightly to moderately cemented sands in earthquake engineering applications. The classification framework proved to be a useful tool for assessing whether the

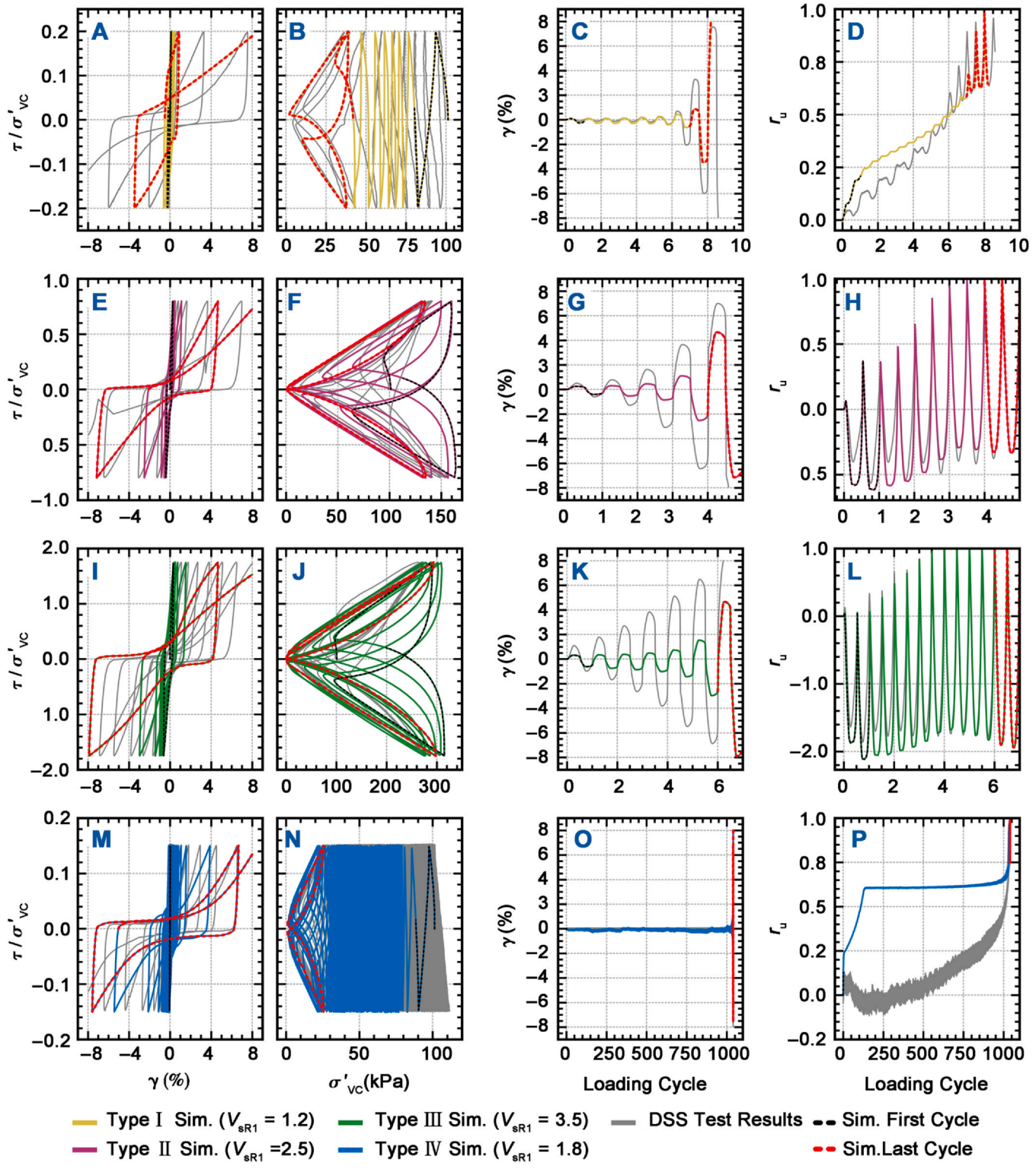


Fig. 4. Comparison of PM4SandC element-level simulations against illustrative cyclic constant-volume DSS test results from Lee (2022), showing for each behavior type: (**A,E,I,M**) Stress-strain response; (**B,F,J,N**) Stress path; (**C,G,K,O**) Shear strain versus loading cycle; (**D,H,L,P**) Excess pore pressure ratio versus loading cycle. Experimental results are shown in gray, simulations are shown in color.

model could replicate the range of observed behaviors across varying cementation levels and loading conditions. Element-level simulations of one illustrative example per behavior type demonstrate that PM4SandC can reasonably reproduce the key features of each behavior type while identifying areas for improvement.

As biocementation continues to mature toward field-scale implementation, frameworks for anticipating and classifying the cyclic response of treated soils will become increasingly important. At the element level, the classification framework presented herein allows practitioners and researchers to anticipate the type of stress path response expected for a given cementation level and seismic demand, which can inform the selection of constitutive model parameters and the interpretation of site characterization data. At the system level, constitutive models calibrated against the observed behavior types

enable numerical assessment of the seismic performance of biocementation treatments across a range of design scenarios. Together, these tools support a coherent workflow from site characterization through element-level response prediction to system-level numerical simulation, which is essential for the responsible deployment of biocementation as a ground improvement strategy for seismic applications.

Conclusions

The following conclusions are drawn from this study:

1) Four distinct types of cyclic stress path response were identified in MICP-treated Ottawa F65 sand subjected to constant-volume DSS loading: Type I (uncemented-like response), Type II (dilative-dominant behavior), Type III (clear evidence of bond breakage), and Type IV (high-cycle fatigue behavior). The pattern exhibited by a given specimen is jointly governed by its cementation level (V_{sR1}) and the applied cyclic stress ratio (CSR).
2) A quantitative behavioral classification framework was developed by establishing four boundaries in V_{sR1}-CSR space: a monotonic failure boundary derived from strain-controlled monotonic DSS tests; a high-cycle fatigue boundary derived empirically from cyclic test results; a phase transformation boundary derived from the monotonic stress path responses; and a bond breakage boundary constrained by both monotonic and cyclic test results. Together these boundaries define a classification process that allows the behavior type of a specimen to be determined from its V_{sR1} and applied CSR.
3) The framework was developed at $\sigma'_{vc} = 100$ kPa for a single sand type and cementation method. The location of the boundaries may shift with consolidation stress, sand type, and cementing agent characteristics, and extending the framework to other conditions represents a natural direction for future work.
4) The four behavior types identified are expected to be broadly relevant to other lightly to moderately cemented sands governed by similar mechanical phenomena, including strain-induced bond degradation and progressive transition toward uncemented-like behavior under loading.
5) The behavioral classification framework was applied as an illustrative example to evaluate the performance of PM4SandC, a plasticity constitutive model for lightly to moderately cemented sands. Element-level simulations demonstrate that PM4SandC can reasonably reproduce the key features of each behavior type, while also identifying areas for further model improvement.

CRediT authorship contribution statement

Luna Laura M. C.: Writing – original draft, Visualization, Investigation, Formal analysis, Data curation, Conceptualization. **Boulanger Ross W.:** Writing – review & editing, Supervision, Investigation, Conceptualization. **Ziotopoulou Katerina:** Writing – review & editing, Supervision, Investigation, Funding acquisition, Conceptualization. **Jason T. DeJong:** Writing – review & editing, Supervision, Investigation, Funding acquisition, Conceptualization.

Declaration of Competing Interest

Jason DeJong is the editorial board member of *Biogeotechnics*, he was not involved in the editorial review or the decision to publish this article. The other authors declare that they have no known competing financial interests or personal relationships that could have appeared to influence the work reported in this paper.

Acknowledgements

The presented study involves work supported by the Engineering Research Center Program of the National Science Foundation under NSF Cooperative Agreement No. EEC-1449501. Any opinions, findings, and conclusions or recommendations expressed in this manuscript are those of the authors and do not necessarily reflect the views of the National Science Foundation.

References

Abdulla, A. A., & Kiousis, P. D. (1997). Behavior of cemented sands—I. Testing. *International Journal for Numerical and Analytical Methods in Geomechanics, 21*(8), 533–547.

Ali Rahman, Z., Toll, D. G., & Gallipoli, D. (2018). Critical state behaviour of weakly bonded soil in drained state. *Geomechanics and Geoengineering, 13*(4), 233–245. https://doi.org/10.1080/17486025.2018.1454608

Bolton, M. D. (1986). The strength and dilatancy of sands. *Géotechnique, 36*(1), 65–78. https://doi.org/10.1680/geot.1986.36.1.65

Boulanger, R. W., & Ziotopoulou, K. (2023). *PM4Sand (Version 3.3) A sand plasticity model for earthquake engineering applications (UCD/CGM-23/01).* Davis: Department of Civil and Environmental Engineering, University of California. https://pm4sand.engr.ucdavis.edu/pm4sand-files.

Burbank, M., Weaver, T., Lewis, R., Williams, T., Williams, B., & Crawford, R. (2013). Geotechnical tests of sands following bioinduced calcite precipitation catalyzed by indigenous bacteria. *Journal of Geotechnical and Geoenvironmental Engineering, 139*(6), 928–936. https://doi.org/10.1061/(ASCE)GT.1943-5606.0000781

Clough, G. W., Iwabuchi, J., Rad, N. S., & Kuppusamy, T. (1989). Influence of cementation on liquefaction of sands. *Journal of Geotechnical Engineering, 115*(8), 1102–1117. https://doi.org/10.1061/(ASCE)0733-9410(1989)115:8(1102)

Consoli, N. C., Cruz, R. C., Consoli, B. S., & Maghous, S. (2012). Failure envelope of artificially cemented sand. *Géotechnique, 62*(6), 543–547. https://doi.org/10.1680/geot.11.P.037

Cuccovillo, T., & Coop, M. R. (1999). On the mechanics of structured sands. *Géotechnique, 49*(6), 741–760. https://doi.org/10.1680/geot.1999.49.6.741

Darby, K. M., Hernandez, G. L., DeJong, J. T., Boulanger, R. W., Gomez, M. G., & Wilson, D. W. (2019). Centrifuge model testing of liquefaction mitigation via microbially induced calcite precipitation. *Journal of Geotechnical and Geoenvironmental Engineering, 145*(10), Article 04019084. https://doi.org/10.1061/(ASCE)GT.1943-5606.0002122

DeJong, J. T., Gomez, M. G., San Pablo, Graddy, C. M. R., Nelson, D. C., ... Kwon, T.-H. (2022). State of the art: MICP soil improvement and its application to liquefaction hazard mitigation. *Proceedings of the 20th ICSMGE-State of the Art and Invited Lectures*.

Festugato, L., Venson, G. I., & Consoli, N. C. (2021). Parameters controlling cyclic behaviour of cement-treated sand. *Transportation Geotechnics, 27*, Article 100488. https://doi.org/10.1016/j.trgeo.2020.100488

Frydman, S., Shaal, B., Baker, R., Steinbach, J., Horn, H., & Hendron, D. (1980). Liquefaction study of cemented sand. *Journal of the Geotechnical Engineering Division, 106*(3), 275–297. https://doi.org/10.1061/AJGEB6.0000933

Gai, X., & Sánchez, M. (2019). An elastoplastic mechanical constitutive model for microbially mediated cemented soils. *Acta Geotechnica, 14*(3), 709–726. https://doi.org/10.1007/s11440-018-0721-y

Gao, Z., & Zhao, J. (2012). Constitutive modeling of artificially cemented sand by considering fabric anisotropy. *Computers and Geotechnics, 41*, 57–69. https://doi.org/10.1016/j.compgeo.2011.10.007

Humire, F., Lee, M., Gomez, M. G., Ziotopoulou, K., & DeJong, J. T. (2022). Development and evaluation of preconditioning protocols for sand specimens in constant-volume cyclic direct simple shear tests. *Geotechnical Testing Journal, 45*(3), 661–673. https://doi.org/10.1520/GTJ20210028

Lade, P. V., & Overton, D. D. (1989). Cementation effects in frictional materials. *Journal of Geotechnical Engineering, 115*(10), 1373–1387. https://doi.org/10.1061/(ASCE)0733-9410(1989)115:10(1373)

Lee, M. (2022). *Biocementation for liquefaction mitigation: Examining response, development, and deployment.* ProQuest One Academic [Doctoral dissertation, University of Washington].

Lee, M., & Gomez, M. G. (2024). Liquefaction triggering and post-triggering behavior of biocemented loose sand. *Canadian Geotechnical Journal, 61*(7), 1331–1352. https://doi.org/10.1139/cgj-2023-0132

Lee, M., Gomez, M. G., El Kortbawi, M., & Ziotopoulou, K. (2022). Effect of light biocementation on the liquefaction triggering and post-triggering behavior of loose sands. *Journal of Geotechnical and Geoenvironmental Engineering, 148*(1), Article 04021170. https://doi.org/10.1061/(ASCE)GT.1943-5606.0002707

Liao, D., Yang, Z. X., Wang, S., & Wu, W. (2024). A hypoplastic model for cemented sand under monotonic and cyclic loading. *Canadian Geotechnical Journal, 61*(5), 915–930. https://doi.org/10.1139/cgj-2023-0079

Lin, H., Suleiman, M. T., Brown, D. G., & Kavazanjian, E. (2016). Mechanical behavior of sands treated by microbially induced carbonate precipitation. *Journal of Geotechnical and Geoenvironmental Engineering, 142*(2), Article 04015066. https://doi.org/10.1061/(ASCE)GT.1943-5606.0001383

Luna, L.M.C., Ham, S., DeJong, J.T., Ziotopoulou, K., & Boulanger, R.W. (2026). A shear wave velocity metric to quantify cementation level and its effect on soil response. [Manuscript submitted for publication].

Luna, L.M.C., El Kortbawi, M., Ziotopoulou, K., Boulanger, R.W., & DeJong, J.T. (2026). Numerical modeling of cemented sands for earthquake engineering applications: formulation, calibration, and validation of PM4SandC, a plane-strain plasticity model. [Manuscript submitted for publication].

Montoya, B. M., & DeJong, J. T. (2015). Stress-strain behavior of sands cemented by microbially induced calcite precipitation. *Journal of Geotechnical and Geoenvironmental Engineering, 141*(6), Article 04015019. https://doi.org/10.1061/(ASCE)GT.1943-5606.0001302

Montoya, B. M., DeJong, J. T., & Boulanger, R. W. (2013). Dynamic response of liquefiable sand improved by microbial-induced calcite precipitation. *Géotechnique, 63*(4), 302–312. https://doi.org/10.1680/geot.SIP13.P.019

Nova, R., Castellanza, R., & Tamagnini, C. (2003). A constitutive model for bonded geomaterials subject to mechanical and/or chemical degradation. *International Journal for Numerical and Analytical Methods in Geomechanics, 27*(9), 705–732. https://doi.org/10.1002/nag.294

Porcino, D. D., & Marcianò, V. (2017). Bonding degradation and stress–dilatancy response of weakly cemented sands. *Geomechanics and Geoengineering, 12*(4), 221–233. https://doi.org/10.1080/17486025.2017.1347287

Rahimi, M., Chan, D., & Nouri, A. (2018). Constitutive model for monotonic and cyclic responses of loosely cemented sand formations. *Journal of Rock Mechanics and Geotechnical Engineering, 10*(4), 740–752. https://doi.org/10.1016/j.jrmge.2018.01.010

Rasouli, H., Fatahi, B., & Nimbalkar, S. (2020). Liquefaction and post-liquefaction assessment of lightly cemented sands. *Canadian Geotechnical Journal, 57*(2), 173–188. https://doi.org/10.1139/cgj-2018-0833

Riveros, G. A., & Sadrekarimi, A. (2020). Liquefaction resistance of Fraser river sand improved by a microbially-induced cementation. *Soil Dynamics and Earthquake Engineering, 131*, Article 106034. https://doi.org/10.1016/j.soildyn.2020.106034

San Pablo, A. C. M., DeJong, J. T., & Carey, T. J. (2024). Influence of biocementation treatment extent on dynamic system performance: A centrifuge liquefaction study. *Soil Dynamics and Earthquake Engineering, 183*, Article 108792. https://doi.org/10.1016/j.soildyn.2024.108792

Saxena, S. K., & Lastrico, R. M. (1978). Static properties of lightly cemented sand. *Journal of the Geotechnical Engineering Division, 104*(12), 1449–1464. https://doi.org/10.1061/AJGEB6.0000728

Sharma, S. S., & Fahey, M. (2004). Deformation characteristics of two cemented calcareous soils. *Canadian Geotechnical Journal, 41*(6), 1139–1151. https://doi.org/10.1139/t04-066

Vranna, A., & Tika, T. (2020). Undrained monotonic and cyclic response of weakly cemented sand. *Journal of Geotechnical and Geoenvironmental Engineering, 146*(5), Article 04020018. https://doi.org/10.1061/(ASCE)GT.1943-5606.0002246

Yu, T., Fleureau, J.-M., Souli, H., & Kong, X. (2024). The improved cyclic resistance of bio-treated sands with various gradations for liquefaction mitigation: Density increase and/or cementation? *Soil Dynamics and Earthquake Engineering, 185*, Article 108894. https://doi.org/10.1016/j.soildyn.2024.108894

Zamani, A., Xiao, P., Baumer, T., Sawyer, B., DeJong, J. T., & Boulanger, R. W. (2021). Mitigation of liquefaction triggering and foundation settlement by MICP treatment. *Journal of Geotechnical and Geoenvironmental Engineering, 147*(10), Article 04021099. https://doi.org/10.1061/(ASCE)GT.1943-5606.0002596

Zhang, A., & Dieudonné, A.-C. (2023). Effects of carbonate distribution pattern on the mechanical behaviour of bio-cemented sands: A DEM study. *Computers and Geotechnics, 154*, Article 105152. https://doi.org/10.1016/j.compgeo.2022.105152

Zhang, H., & Zhang, X. (2024). A state-dependent dilatancy model for cemented sand. *Computers and Geotechnics, 173*, Article 106527. https://doi.org/10.1016/j.compgeo.2024.106527

Zhao, H., Zhou, A., Shen, S.-L., & Arulrajah, A. (2025). A bottom-up hierarchical model for MICP-treated soil based on DEM. *Computers and Geotechnics, 185*, Article 107345. https://doi.org/10.1016/j.compgeo.2025.107345